International Journal of Adhesion & Adhesives 117 (2022) 103013

Contents lists available at ScienceDirect

International Journal of Adhesion and Adhesives

journal homepage: www.elsevier.com/locate/ijadhadh

Self-healing capability of novel eco-epoxy adhesives based on the modified tannic acid on Al adherends tested in a single lap joint

Nataša Z. Tomić [a,*], Mohamed Nasr Saleh [b,c], Milad Saeedifar [b], Aleksandar Marinković [d], Sofia Teixeira de Freitas [b,**]

[a] Innovation center of Faculty of Technology and Metallurgy in Belgrade ltd, Karnegijeva 4, Belgrade, Serbia
[b] Structural Integrity & Composites Group, Faculty of Aerospace Engineering, Delft University of Technology, the Netherlands
[c] Advanced Materials Research Center, Technology Innovation Institute, Masdar City, Abu Dhabi, United Arab Emirates
[d] Faculty of Technology and Metallurgy, University of Belgrade, Karnegijeva 4, 11070, Belgrade, Serbia

ARTICLE INFO

Keywords:
Self-healing
Adhesion
Eco-epoxy
Tannic acid
Acoustic emission

ABSTRACT

The aim of this paper is to study the self-healing capability of fractured Al joints bonded with novel eco-epoxide adhesives synthesized from a bio-renewable raw material (tannic acid – TA). Two synthesized eco-epoxy components based on TA, (A) glycidyl ether and (B) glycidyl phosphate ester of TA, were used as a replacement for the toxic epoxy component based on Bisphenol A. The effect of the eco-epoxy components on the self-healing capability was measured as a recovery of shear strength in a single lap joint (SLJ) test after complete failure, which was compared to the reference epoxy (R). The self-healing procedure was performed in an autoclave at 180 °C for 2 h and 2 bars. A combination of two monitoring techniques, Digital Image Correlation (DIC) and Acoustic Emission (AE), was used to monitor the strain distribution and damage propagation in the SLJ. The measured shear stress of A and B adhesives in the SLJ had values in the range of 2.3–5.1 MPa. A fracture analysis showed complete adhesive failure for all the tested adhesives, which was not affected by the self-healing process. Out of all adhesives, only the A adhesive demonstrated the capability to heal. The recovery of the shear strength for adhesive A was higher than 50% of the virgin case. In addition, the AE analysis managed to capture a clear distinction between the signals for the virgin and the self-healed tests for adhesive A. Results obtained in this study highlighted the promising potential of using bio-based epoxy adhesives in structural adhesive bonding with the possibility of using self-healing in the recovery of the strength of such bonded joints.

1. Introduction

Polymers are widely employed in a variety of sectors today, including transportation, electronics, stationery, sports equipment, and civil engineering [1]. Deep microcracks in the structure can be caused by mechanical, thermal, chemical, UV radiation, and other factors, leading to deformation or disintegration. Traditional repair approaches fail to restore hidden microcracks inside the system over the service life of such polymeric components. Self-healing polymeric materials were developed in the 1980s as a way to repair undetectable microcracks and extend the stability and service life of polymerized components [2]. In theory, self-healing polymer materials have the potential to regain a significant amount of load transfer capability after being damaged. This form of healing might happen on its own or as a result of a treatment (such as radiation, heat, and water). As a consequence, these solutions should improve the integrity and protection of polymeric components while reducing the need for costly active inspection or external service [3]. As a result, the need for self-repairing materials is increasing. Until recently, the bulk of self-healing materials have been produced from petroleum, and existing research has largely focused on their healing abilities [4–7]. Scientists' focus has switched to green and ecologically sustainable biomass products as fuel supplies grow scarce and the climate deteriorates. Polymer materials have also been developed using redundant bio-sources such as sodium alginate, proteins, chitosan, cellulose, and natural rubber [8]. A bio-based substance is made using components derived from living (or formerly alive) organisms. Until now, the self-healing mechanisms of bio-based polymers have been divided into two categories: i) the usage of healing agents [9,10], and ii)

* Corresponding author.
** Corresponding author.
E-mail addresses: ntomic@tmf.bg.ac.rs (N.Z. Tomić), S.TeixeiraDeFreitas@tudelft.nl (S. Teixeira de Freitas).

https://doi.org/10.1016/j.ijadhadh.2021.103013

Available online 5 October 2021

intrinsic healing via the reversible chemical bonds [11].

One of the most serious issues in the field of adhesively bonded joints is the repair process. Even though adhesive bonding provides the best load transfer and structural performance, adhesives have mostly been restricted to secondary structures due to concerns about bonded joints' fatigue and durability throughout their structural lifetime [12], as well as the challenges of testing a bond line after manufacture and during operation [13]. Self-healing adhesives with a longer lifespan and lower maintenance costs might alleviate both problems. Self-healing epoxy adhesives in the bonding of structural materials such as steel and aluminum are the subject of very few studies (Al) [14,15]. The micro-encapsulation approach, which is frequently hazardous, costly, and time-consuming, is used in the majority of these research projects.

Adhesive bonds are primarily intended to function in a condition of shear, in which forces apply parallel to the adhesive's cross-section in opposing directions of its plane [16]. When a bonded component is built properly, shear testing is performed to evaluate the maximum stresses that it can withstand. The single-lap joint (SLJ) shear test is frequently utilized in the automotive and aerospace industries because it is simple to prepare, cost-effective, and practical [17,18]. Although self-healing of bulk polymers has been achieved, there has been relatively little research on the self-healing of polymeric adhesives. As a result, it's worth looking at the joints that these materials form to learn more about how they may be used as adhesives.

The goal of this study is to investigate the potential of fractured Al joints to heal when bonded with novel eco-epoxide adhesives synthesized from a bio-renewable raw material (tannic acid – TA). Therefore, this study proposes a new repair method of adhesively bonded joints based on the intrinsic healing capability of TA. The healing efficiency was determined as maximal load recovery after a complete failure in the SLJ test. Other methods used in investigating the self-healing phenomenon of TA-based epoxy adhesives are acoustic emission (AE) and digital image correlation (DIC). Demonstrating the excellent healing effectiveness of bio-based adhesives in the bonding of lightweight structures can boost faith in the relevance of bio-based adhesives in structural bonding.

2. Materials and manufacturing

2.1. Adhesives and adherends

Chemicals used in this study for modification of TA are sodium hydroxide (NaOH, ACS reagent, ≥97.0%, pellets), epichlorohydrin (EPH, ≥99.0% (GC) for synthesis), *N*-methyl-2-pyrrolidone (NMP, ≥99.7% (GC)), phosphorus oxychloride ($POCl_3$, ReagentPlus® 99%), deionized water (MiliQ), chloroform (anhydrous, ≥99%), magnesium sulfate (p.a., drying agent, anhydrous, ≥98.0% (KT), powder (very fine)), tetrahydrofuran (THF, ACS reagent, ≥99.0%), (±)-Glycidol (96%), and calcium chloride (anhydrous, powder, ≥97%), which were used as received from Sigma Aldrich, USA. The solvent used for surface cleaning, acetone (technical grade), was supplied from Sigma Aldrich, USA. Reference adhesive was selected to be BPA-based epoxy (LG700 epoxy component and HG 700R curing agent) was supplied from GI-NI ltd, Belgrade, Serbia (epoxy value 0.62, T_g = 79.4 °C). The substrate selected was Al alloy 2024, supplied from Salomon's Metalen, the Netherlands.

2.1.1. Modification of tannic acid

2.1.1.1. Synthesis of glycidyl ether of TA. The modification of TA was performed in the reaction of TA and EPH, in order to introduce reactive epoxy groups that can react in the epoxy system. The detailed synthesis can be found in the literature [19]. The obtained product was highly viscous brownish oil with the appearance presented in Fig. 1.

2.1.1.2. Synthesis of glycidyl phosphate ester of TA. The modification of TA was performed in the reaction of TA with $POCl_3$ and glycidol, in order to introduce reactive epoxy groups that can react in the epoxy system. The detailed synthesis can be found in the literature [19]. The obtained product was highly viscous light brownish oil with the appearance presented in Fig. 1.

The chemical structure of both types of adhesive components obtained by modification of TA is presented in Fig. 1.

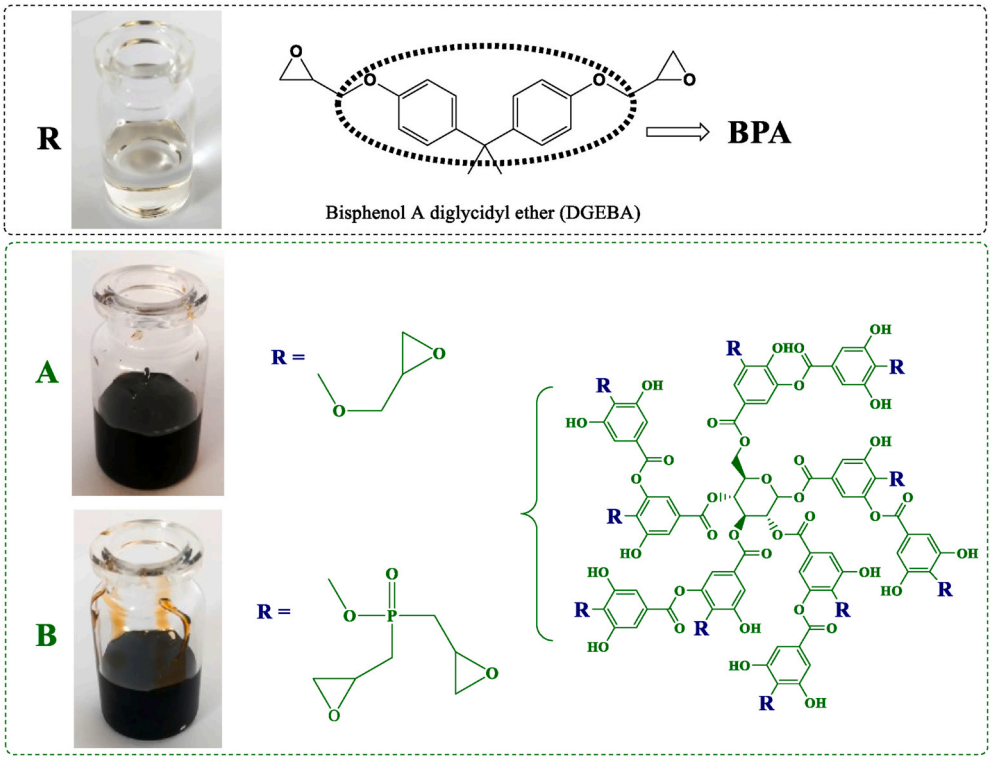

Fig. 1. Schematic representation of studied adhesives and employed type of TA modification.

2.2. Surface pretreatments and bonding

The surface preparation of aluminum samples before bonding was as follows: I step – solvent cleaning (acetone), II step – mechanical treatment – grit blasting with Al_2O_3 powder (Corublast Super Z-EW No. 40, Ø 0.35–0.50 mm), III step – solvent cleaning (acetone) and IV step – physical removal of contaminants and drying – air blow duster gun.

Three types of adhesives were used for the SLJ test: 1) reference epoxy adhesive (R); 2) epoxy adhesive with 15 wt% of glycidyl ether of TA (adhesive A); and 3) epoxy adhesive with 15 wt% of glycidyl phosphate ester of TA (adhesive B). Glass bead spacers (150–250 μm), used for the thickness control of adhesive layer, were mixed with the adhesives at 0.1 wt% before bonding. Adhesive R was made with a weight mixing ratio LG700:HG 700R = 100:30. Bonding of Al specimens was done at room temperature for 24 h, with post-curing on 70 °C for 4 h. The dimensions of specimens were 125 × 25 mm with 6 mm thickness. The overlap area was 50 × 25 mm (see Fig. 2).

3. Experimental procedure

The experimental procedure was methodically planned to address all of the essential aspects and achieve the research study's goals. The DSC study is the first stage in this methodical approach to determining: i) if the synthesized adhesives can react chemically, showing their self-healing capability, and if so, ii) what the healing process parameters, such as temperature and time, should be. The FTIR analysis was then performed, which should offer enough information regarding the structural modifications that occurred throughout the healing process, as well as what these changes might mean. Finally, the DMA analysis was critical for determining/quantifying the impact of such changes, as detected by the FTIR, on the bulk adhesive's mechanical characteristics. To put it more simply, to figure out how these changes are reflected mechanically. Despite the knowledge gained from this methodical approach, there is still a gap in understanding since these approaches are incapable of capturing changes at the adhesive joint level, which is the focus of this work. Therefore, it was critical to validate the self-healing concept utilizing SLJ testing. In addition, during the SLJ testing, in-situ NDT methods such as DIC and AE were used to confirm and capture any differences between the virgin and healed specimens. Each of the approaches is described in the subsections below in the same planned sequence.

3.1. Physical and chemical characterization

3.1.1. FTIR analysis

FTIR spectroscopy of epoxy components used in adhesive preparation was performed to confirm obtained structure of synthesized components and to compare the presence of functional groups that can affect the bonding interface. Analysis was done using a Nicolet™ iS™10 6700 spectrometer (Thermo Scientific) in the attenuated total reflectance (ATR) mode with a single bounce 45 °F Golden Gate ATR accessory with a diamond crystal, and DTGS detector. FTIR spectra were obtained at 4 cm^{-1} resolution with ATR correction. The FTIR spectrometer was equipped with OMNIC software and recorded the spectra in the wavelength range from 2.5 μm to 20 μm (i.e., 4000 –500 cm^{-1}).

3.1.2. DSC analysis

Differential scanning calorimetry (DSC) is a method for measuring heat flows and temperatures associated with material thermal transitions. The method can be used to assess a variety of material properties, including glass transition temperatures, melting and crystallization cases, phase transitions, cure kinetics, and oxidation, and other chemical reactions. Used epoxy adhesives and bio-based components were tested by the DSC technique to investigate the self-healing capability and

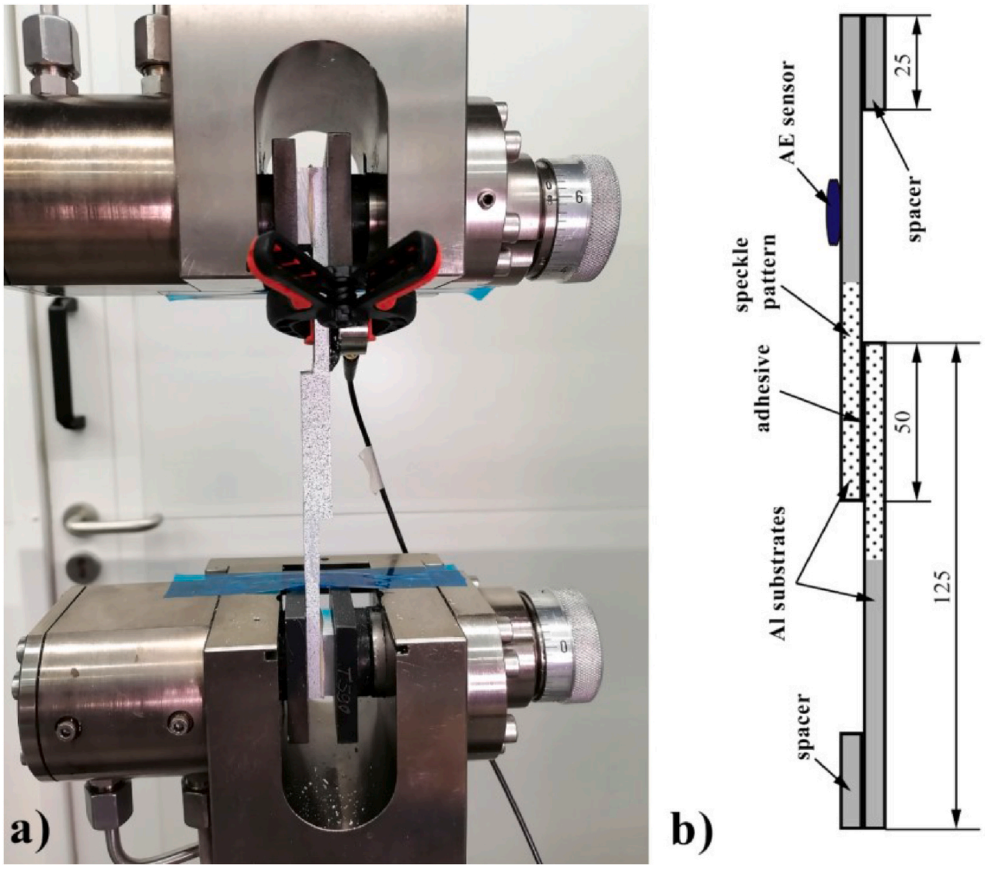

Fig. 2. a) SLJ test setup and b) schematic of the specimen (all the dimensions are in mm).

healing temperature. DSC analysis was performed on DSC250, TA Instruments, in a temperature range of 20–200 °C, under an N_2 atmosphere, in Tzero Al hermetic pans with a sample mass of 6.6 ± 0.4 mg. The first run was performed with a heating rate of 10.00 °C/min to 200.00 °C, then the sample was cooled down with a rate of 5.00 °C/min to 20.00 °C, and the second run was repeated like the first one. TRIOS Software from TA Instruments was used for T_g determination and calculation of associated enthalpies for all tests.

3.1.3. DMA analysis

Dynamic mechanical analysis (DMA) is an important extension of thermal analysis because it can show fine temperature transitions that influence the material's complex modulus. DMA samples were prepared according to the procedure described in section 2.2. The mixing weight ratio was LG700:HG 700R = 100:30. In the case of adhesive A and B, the 15 wt% of LG700 was replaced with glycidyl ether of TA and with glycidyl phosphate ester of TA, respectively. They were cast in a Teflon mold, cured at room temperature for 24 h, and post-cured at 70 °C for 4 h. The dimensions of specimens were 60 × 10 mm with 2 mm thickness. The visco-elastic analysis of used epoxy adhesives was performed by PerkinElmer Diamond DMA RSA-G2 in a tension fixture (rectangle), at the temperature range 25–200 °C, heating rate 1 °C/s, and angular frequency of 1 Hz. The glass transition temperature (T_g) was calculated as the maximum of tan $\delta(T)$ curve and denoted as $T_{g(\tan\delta \text{ peak})}$.

3.2. Mechanical testing

3.2.1. Single-lap joint (SLJ) testing

The shear strength of single-lap-joint of bonded Al specimens using eco-epoxy adhesives was tested by tension loading in a Zwick Roell machine equipped with a 10 kN load cell and hydraulic grips to minimize the slippage due to gripping – see Fig. 2. All the specimens had the same nominal dimensions (25 mm wide and 6 mm thick) and overlap area (25 × 25 mm^2). For each specimen group, five specimens were tested in order to ensure the reproducibility and repeatability of the results. SLJ test was monitored by combined in-situ monitoring techniques such as DIC and AE.

After the destructive mechanical tests of the virgin samples, the samples were re-joined at elevated temperatures. The test procedure was repeated to evaluate the self-healing capability of novel bio-based adhesives.

Thus, four different test procedures were performed:

1) Complete fractured of the virgin specimens, which were denoted by the used adhesives as R, A and B
2) Self-healed of completely fractured specimens, denoted as R–H, A-H and B–H

3.3. In-situ monitoring techniques

3.3.1. Digital image correlation (DIC)

In order to visualize the strain contour map ahead of the crack tip [20,21] and measure the crack length throughout the test [22], a two-dimensional (2D) DIC system (see Fig. 2) was used. The DIC system consisted of an 8-bit "Point Grey" camera with a resolution of 5 MP, equipped with a "XENOPLAN 1.4/23" lens. The software used for capturing and recording the speckle pattern images was ViC-Snap 8, a product of "Correlated Solutions Inc.". The acquisition rate of 1 and 0.33 frames per second (fps) was used for the initial and reloading tests respectively. Afterward, the acquired images by ViC-Snap 8 were processed using ViC-2D 2009 software. For processing, the subset size was set to 20 × 20 pixels with a step size (distance between subsets) of 5 pixels. The observation window of approximately (650 × 650) mm^2 produced an image with dimensions of (2048 × 2048) pixels.

3.3.2. Acoustic emission (AE)

In order to record produced AE signals during the SLJ test, one AE sensor was placed on the top Al surface of the specimen (see Fig. 2). The AE sensor was broadband, resonant-type, and single-crystal piezoelectric transducer from Vallen Systeme GmbH, AE1045SVS900 M, with an external 34 dB pre-amplifier and an operating frequency range of [100–900 kHz]. An AMSY-6 Vallen, an 8-channel AE system with a sampling rate of 2 MHz, was used to record the AE signals. Ultrasound gel was applied between the surfaces of the sensor and the specimen to ensure good acoustical coupling. The AE threshold was set as 40 dB.

3.4. Self-healing procedure

Tested samples from SLJ (completely fractured) were subjected to self-healing treatment at 180 °C and pressure of 2 bars (1 from the vacuum and 1 of pressure) in a Scholtz Autoclave. The heating temperature rate was 3 °C/min, the dwell time 2 h, and the cooling rate was 3 °C/min.

3.5. Surface characterization

Post-mortem fractured surface of representative samples from each tested group was analyzed using a 3D optical microscope with a wide-area 3D measurement system, type VR-5200 from Keyence, USA.

4. Results and discussion

4.1. Physical characterization

4.1.1. DSC analysis

The self-healing potential of the utilized adhesives, as well as the structural changes that happened throughout the self-healing treatment, were investigated using DSC analysis. Fig. 3 illustrates the DSC findings obtained in the two runs adhesives R, A, and B since samples had the same previous thermal history (i.e. they were cast, cured, and tested simultaneously). Adhesive R exhibited the lowest glass transition temperature (T_g) of all the tested adhesives in the first run, at 63 °C (Fig. 4a). In the first run, both A and B adhesives had T_g = 70 °C (Fig. 3b and c). T_g is higher for A and B than for R due to the stronger limitation of polymer chain rotation movements caused by higher reactivity and a larger quantity of accessible epoxy groups, resulting in higher cross-linking density [23]. The exothermic reaction was also seen in the first run for all samples, with a peak temperature of ~175 °C. The exothermic region refers to high-temperature curing, i.e. homopolymerization of leftover epoxy groups that remained owing to the use of less hardener to increase the system's self-healing capabilities. The onset temperature of the exothermic peak was: R – 107 °C, A – 119 °C and B – 129 °C. The T_g, or the amount of the restriction of polymer chain movement required for the polymerization reaction to occur, influences the difference in onset temperature. The greater number for B than for A is since molecule B is larger/bulkier, as well as having a higher quantity of hydrogen bonding. Between polymer chains, hydrogen bonds function as anchors, limiting mobility and delaying the initiation of exothermic reactions [24]. When comparing adhesive A (9.65 J/g) to adhesive B (4.95 J/g) and R (7.64 J/g), adhesive A had the greatest enthalpy. The number of chemical bonds formed increases as the enthalpy increases. When compared to R and B, adhesive A had the strongest reactivity at high temperatures. Fig. 4 shows/details potential self-healing processes using adhesives R, A, and B at high temperatures. Aside from epoxy group homopolymerization (adhesive R), the interaction between the phenolic groups of TA and epoxy can also occur (A and B) [25]. The remaining phenolic groups of TA and hydroxyl groups of DGEBA in A are both accessible, but access to phenolic groups in B is sterically blocked by the glycidyl phosphate functional groups, as shown in the schematic. Apart from the steric barrier, the mobility of bulky modified TA molecules in cured adhesive B is significantly lower than in A, making self-healing much more difficult.

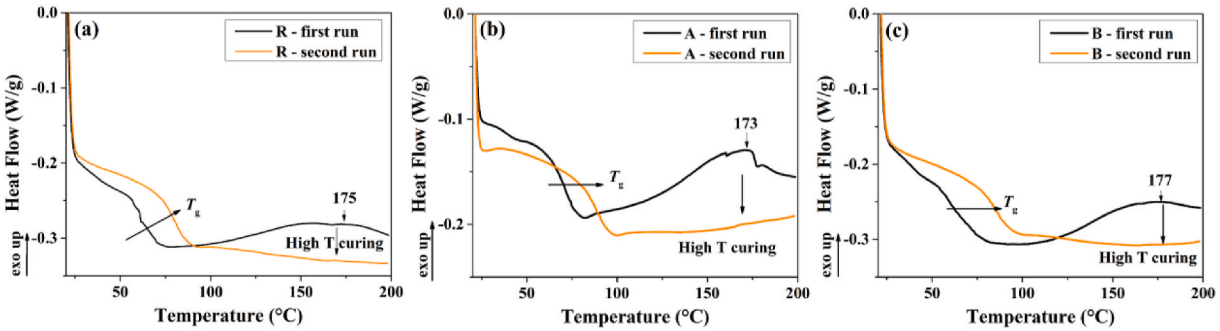

Fig. 3. DSC runs for adhesives: (a) R, (b) A and (c) B.

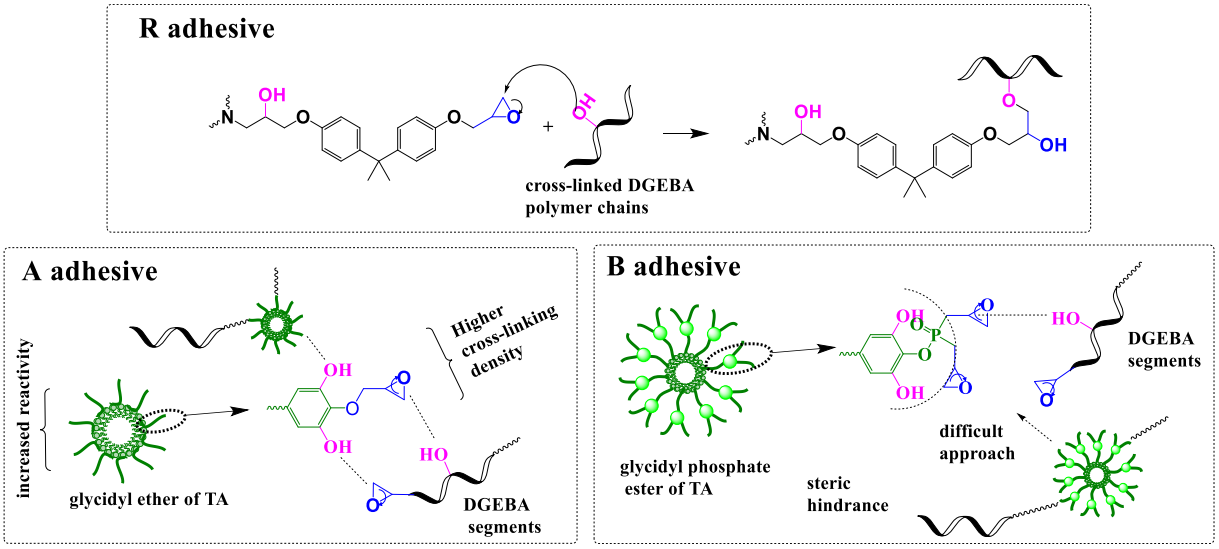

Fig. 4. Possible theoretical reactions in a self-healing process at high temperatures of adhesives R, A and B.

The lowest enthalpy of cross-linking of all adhesives was due to these processes in B.

Fig. 3 shows that the following heating to 200 °C, no sample displayed exothermic reactions in the second DSC run, indicating that the all cross-linking reactions already took place in the first run. An improvement in T_g for about ~16 °C was found for all examined adhesives, having values of T_g (R) = 79.11 °C (Fig. 3a), T_g (A) = 87.78 °C (Fig. 3b) and T_g (B) = 85.18 °C (Fig. 3c). These findings showed that adhesive A may self-heal at elevated temperature owing to the glycidyl ether of TA. Up to 180 °C, the bulk of exothermic reactions took place. The temperature of the self-healing process was chosen to be 180 °C because the phenolic and aliphatic hydroxyl groups react with residual epoxy groups between 115 and 180 °C [25]. Because the DSC testing method took roughly 1 h, it was considered that a self-healing process should take at least 2 h. Despite this, the DSC study revealed that adhesives have a residual reactivity at high temperatures and that adhesive A has a strong capacity for healing.

4.1.2. FTIR analysis

Fig. 5 shows the FTIR spectra of adhesives R, A, and B on virgin and self-healed samples. The spectra of DGEBA resin cured with isophorone diamine (IPDA) hardener are shown in Fig. 5a. Stretching vibrations of hydroxyl groups (O–H) are responsible for the wide peak at ~3400 cm^{-1}. Aromatic C–H stretching vibrations were predicted at ~2962 cm^{-1}, however, they were overlapped with the symmetric and asymmetric vibrations of methyl (CH_3) and methylene (CH_2) groups at 2926

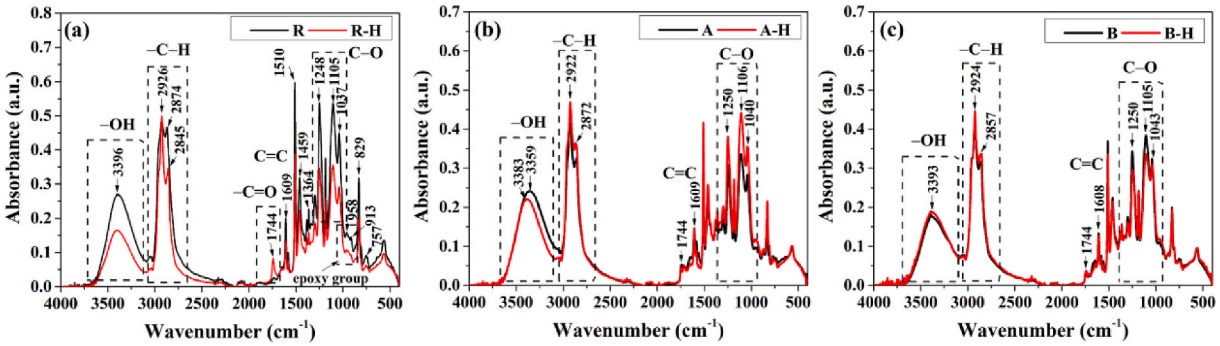

Fig. 5. FTIR spectra of adhesive samples, both virgin and self-healed: (a) R, (b) A and (c) B.

cm^{-1} and 2874 cm^{-1}, respectively. At 1609 cm^{-1}, the distinctive C=C stretching of the benzene ring found in DGEBA's bisphenol A is visible. The symmetrical and asymmetrical C–H in-plane bending vibrations of CH_3, were observed at 1364 cm^{-1} and 1459 cm^{-1}, respectively. The peaks at 1248 cm^{-1} and 1105 cm^{-1} are C–O stretching vibrations, whereas the peak at 1037 cm^{-1} is C–O stretching in the modified epoxy resin's molecular backbone, which includes the anisole-like moiety [26]. The epoxy groups whose intensity diminishes throughout the curing operations correspond to the vibration bands at 958, 913, and 757 cm^{-1} [27]. At 830 cm^{-1}, the C–N stretching vibration was found, which corresponds to the main aliphatic amine employed as a curing agent in epoxy resin [28].

Epoxy resin peaks were also seen for adhesives A and B, with the difference being due to the TA component (Fig. 5b and c). Due to the ester connections of the TA core, the carbonyl group vibration at 1744 cm^{-1} was observed in both virgin samples of A and B [19].

After the self-healing process (R–H), the FTIR spectrum of adhesive R shows structural changes (see Fig. 5a). At 1744 cm^{-1}, the primary changes can be seen in the vibration of the hydroxyl and epoxy groups, as well as the emergence of carbonyl group vibration. Because of the epoxy resin homopolymerization seen in Fig. 4 for adhesive R, a reduction in the quantity of both epoxy and –OH groups was anticipated. The presence of the carbonyl group vibration is linked to the occurrence of a thermo-oxidation process [29]. The thermo-oxidation process can result in chain scission and the appearance of double bonds, carbonyl, and amide species/moieties, as shown in the DGEBA/IPDA system [30,31]. Carbonyl groups can also be formed via the oxidation of secondary hydroxyl groups in cured epoxy resin [32]. Following this kind of oxidation, the strength of the C–O band vibration at 1248 cm^{-1}, which is characteristic of secondary alcohols, decreases, as seen in R–H spectra in Fig. 5a. Scheme 1 depicts two potential routes for the thermo-oxidation of DGEBA, including the production of the carbonyl group.

Both paths include the production of the carbonyl group, as shown by the emergence of a peak at 1744 cm^{-1} in Fig. 5a, based on the bonds broken and created. Both of them also contain the breaking of the C–H bond, as evidenced by a drop in peak intensity at 2874 cm^{-1} and a shift to a lower wavenumber, namely 2845 cm^{-1}. Only route (I) addresses the breaking of the O–H bond, which can cause a decrease in peak intensity at 3396 cm^{-1} to some extent. The yellowing of the sample was caused by the development of carbonyl groups on the DGEBA backbone. The mechanism of the carbonyl group development in the polymer backbone induced by the oxidation process has been documented to generate yellowing in other polymers besides DGEBA [33,34].

Adhesive A's self-healing process resulted in structural alterations such as a decrease in O–H peak intensity and an increase in C–O peak intensity (see Fig. 5b). These modifications are consistent with the idea that phenolic groups are involved in cross-linking reactions during the self-healing process (see Fig. 4). The absence of carbonyl group formation in the A-H sample is related to the introduction of modified TA, which enhanced thermal stability and thermo-oxidative resistance [35,36].

In comparison to virgin adhesive B, the B–H sample's FTIR spectrum exhibited practically no structural changes following the self-healing process (see Fig. 5c). Minor rearrangements of C–O groups owing to the relaxing process of polymer chains or leaching of oxygen-containing chemicals might explain a modest reduction in the strength of C–O stretching vibrations. Epichlorohydrin was shown to be the most often leached component in DGEBA epoxy resins [29].

The residual reactivity of the investigated adhesives was determined via FTIR analysis, with R and A had the highest residual reactivity, indicating the possibility of self-healing. Furthermore, the presence of the modified TA resulted in increased thermal stability.

4.1.3. DMA analysis

The chemical composition of synthesized macromolecules, cross-linking density, polymer chain interaction, and the effect of TA modification on polymer chain mobility and phase formation are all significant characteristics of adhesives. The DMA was therefore utilized to investigate the performance of the new bio-based adhesives as well as the impact of the TA component on their characteristics. Fig. 6 depicts the DMA findings, which include the damping factor (tanδ), temperature dependency of the storage modulus (G'), and loss modulus (G''), which indicate the elastic and viscous behavior of the adhesives investigated, respectively. Table 1 shows the G'_{GS} and G'_{RP} values for glassy state and rubbery plateau at 30 °C and 200 °C respectively. By comparing the glass transition temperature (T_g), which was calculated as the maximum of tan $\delta(T)$ curve ($T_{g(\tan\delta\ peak)}$), the influence of the additional TA component on the polymer network structure was examined. The height of the peak on the tan$\delta(T)$ curve (tanδ height) and the width of the peak on the tan $\delta(T)$ curve (tanδ width), which was calculated as the whole width at half maximum, were both investigated. The storage modulus in the rubbery state (G'_{RP}) is used to estimate the cross-linking density (ν) of the adhesives in the following way [37]:

$$\nu = \frac{G'_{RP}}{RT} \tag{1}$$

where R is the universal gas constant and T (K) = T_g (K)+ 30.

Fig. 6 depicts the curves that depict samples transitioning from a glassy to a rubbery state, or α-relaxation, as a function of polymer chain segmental motion. The glass transition temperature is indicated by the damping factor curves (tan$\delta(T)$) in Fig. 6a. When compared to the DSC findings, there was a substantial difference in T_g (see Fig. 3). This distinction highlights the fact that DMA is more sensitive to polymer transitions than standard thermal analysis methods like DSC [38]. In extensively filled/reinforced materials, for example, T_g detection by DMA is simpler since the modulus increases by many orders of magnitude in the T_g area, whereas the heat capacity (the foundation of T_g detection in DSC) changes less [38]. Furthermore, since DMA is so

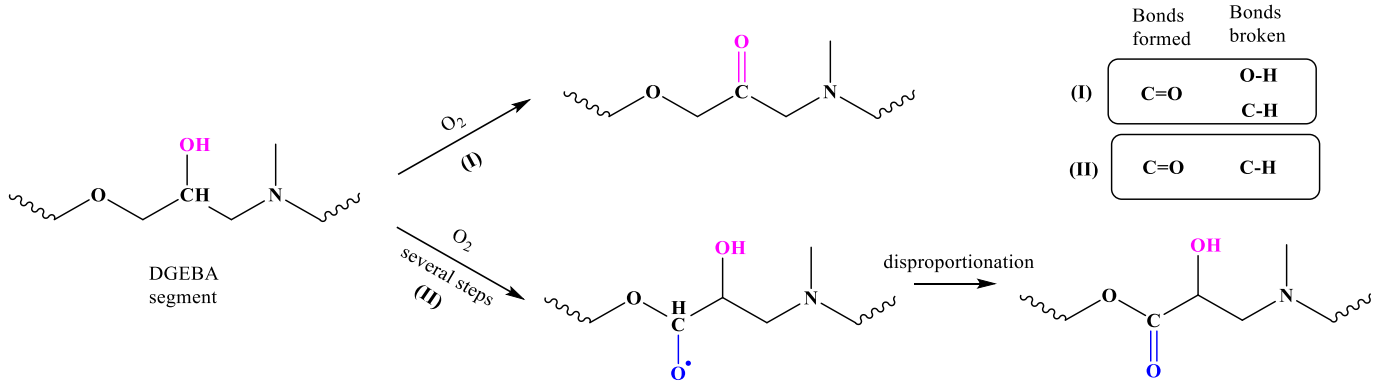

Scheme 1. Carbonyl formation reaction on DGEBA reactive sites containing the i-propanol moiety [29].

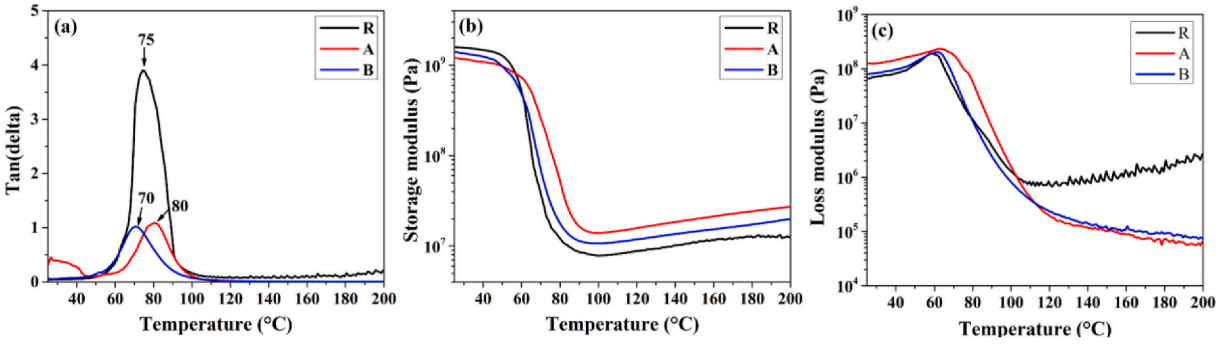

Fig. 6. Analyses of the tested adhesives R, A, and B using DMA are shown as: (a) tan (delta), (b) storage modulus, G' and (c) loss modulus, G''

Table 1
Results of DMA analysis of studied adhesives.

Sample	$T_{g\ (tan\delta\ peak)}$ (°C)	tanδ height	tanδ width [°C]	G'_{GS} (GPa)	G'_{RP} (MPa)	$\nu \cdot 10^3$ (mol/cm^3)
R	75	3.900	17.47	1.56	12.49	4.315
A	80	1.091	20.96	1.10	27.12	9.237
B	70	1.022	19.92	1.31	19.89	6.972

sensitive, it may detect weak secondary transitions in polymers such as alpha and beta transitions that are not obscured by background noise or other interferences. However, in some cross-linked thermosets or heterophase polymers, the glass transition area is so large that neither the peak of the loss modules nor tan can provide correct T_g values [39]. The cross-linking density has a significant impact on the glass transition and the appearance of the tanδ curve. Low damping factor (tanδ) values in the tan$\delta(T)$ curve for adhesives A and B indicate that the generated polymer network had a higher cross-linking density than adhesive R [40]. The estimated cross-linking density (ν) values from Table 1 reveal that adhesive A has more than double the cross-linking density of adhesive R (114%). Adhesive B has a ν of 62% more than adhesive R. Thus, the transition loss dispersion reduces in intensity, broadens, and switches to higher temperatures as the cross-linking density increases. Furthermore, when the crosslinking density increases, the storage modulus slope lowers. When comparing adhesives A to R and B, the enhanced storage modulus in the rubbery area is attributable to the restriction of free movement of the polymer chains due to the higher cross-linking density (Table 1) [41]. The loss modulus peak showing the glass transition has slightly lower T_g values than predicted [39], although adhesive A has the highest T_g value. Because of the greatest T_g value and cross-linking density, the DMA results may imply that bulk adhesive A has improved mechanical characteristics.

4.2. Mechanical characterization and in situ monitoring

Five specimens were tested for each adhesive type and the response was found to be very repeatable. Thus, a representative specimen from each adhesive type (A, B and R) is depicted in Fig. 7 for the sake of the discussion along with AE data. The macroscopic response can be divided into two sections: a linear section up to ~0.8 mm and 4 kN followed by a non-linear section mainly for adhesive B and R specimens. This non-linear behavior cannot be justified in the light of the adherend yielding as the aluminum stripes used were 5 mm thick and such load level (4 kN) is not sufficient to exceed the yield strength of aluminum. However, this non-linear behavior can be associated with possible slippage at the gripping region that occurred beyond that load level as indicated in Fig. 7 with the horizontal dashed line. This slippage hypothesis can be confirmed with the AE RMS data response (see Fig. 7a). It is very clear that for both adhesive B and R specimens, there exists a dwell region correlating accurately with the non-linear segments observed in the load-displacement curves. The RMS is calculated as the root mean square of the AE signals in specific time intervals that indicate the severity of the AE activities. As it is clear, from the beginning of the test up to a displacement of ~0.6 mm, there are some AE signals with RMS values less than 5 μV that can be related to the micro-damage formation in the adhesive material or elastic deformation of the adhesive and adherends. Once, the displacement crosses the limit of 0.6 mm, the RMS value of the signals increases significantly. In the case of adhesive A, this instantaneous increase of the RMS refers to the macroscopic damage in the adhesive which leads to the final failure of the specimen. While, in the case of adhesives R and B, the instantaneous increase trend is then followed by a low-level constant RMS trend which is correlated to the slippage of the specimen. Therefore, in the case of

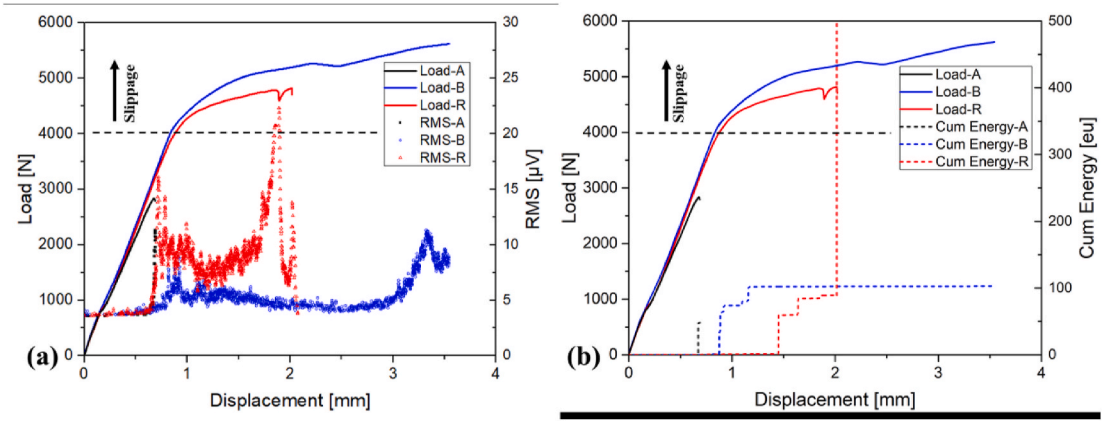

Fig. 7. Virgin representative load-displacement curves with AE features: a) RMS and b) Cum. Energy.

these two adhesives, the initiated macroscopic damage could not propagate throughout the joint, because of the slippage of the specimen. Afterward, the RMS value increases again towards the end of the test, which is due to the final failure of the joint. Cumulative AE energy curves are consistent with the RMS curves, in which the AE energy of the early-stage signals is negligible compared to the AE signals that originated close to the final failure of the specimens. This sharp increasing trend in the cumulative energy curves towards the final fracture indicates the brittle fracture nature of the adhesives.

One very important aspect to investigate in adhesively-bonded joints in general and SLJs, in particular, is the peel and shear strain/stress components. Using DIC enables capturing such information. Thus, Fig. 8a and b depict the peel (ε_{xx}) and shear (ε_{xy}) strains distributions along the bondline of the virgin SLJ specimens at a specific load level which is common in all specimens (~2.5 kN) and also before experiencing any slippage as previously highlighted. The centerline of the specimens is considered as (y = 0) with the positive and negative directions indicated on the representative specimen. For both peel and shear strains, the distribution along the bond line represents a typical distribution with the peaks located at the discontinuities at the two edges, however the distribution is not perfectly symmetric. This observed asymmetry can be attributed to the load introduction during testing as the top grip (y > 20 mm) was the stationary one while the bottom grip (y < −20 mm) was the movable one, leading to higher strain intensity at the edge closer to the stationary grip. A similar observation was reported by Kupski et al. [42,43] for CFRP single-lap bonded joints. However, adhesive A experiences a larger peak along with a shift in the y-direction along the bond line. This can be associated with the fact that the 2.5 kN chosen point is very close to the final failure which means that the crack started propagating from the edge towards the center of the specimen spanning the full length of the bonded region.

After the healing process, only adhesive A specimens were found to be bonded. Both adhesive B and R specimens were easily open just during handling before the test. Even if some weak mechanical bonds were formed for B and R adhesive specimens, they were not strong enough to hold the specimen intact. Comparing the load-displacement response of the virgin and the healed adhesive A specimens (see Fig. 9) suggests that healing was very successful resulting in a minor reduction/loss in stiffness of (<10%) while the reduction in the ultimate load is almost (50%). In other words, the healing efficiency, calculated as the ratio between the healed vs. the virgin cases, from stiffness and ultimate load point of view is 90% and 50% respectively. Another important observation is the change of slope of both the virgin and healed specimens at ~0.2 mm. This can be due to specimen adjustment in the grips during the testing as indicated previously and observed by Hodgkinson et al. [44]. The same observation was noticed for the virgin testing regardless of the adhesive type, which confirms that it is not a material property or response. The RMS and cumulative AE curves of the healed specimen are different from the virgin specimen. The healed specimen has more AE events, which are generated at earlier stages in the testing, indicating the weaker mechanical bonds formed during the healing process. In this way, the damage is relatively more progressive, unlike the virgin case that experiences much fewer AE signals and is mainly concentrated towards the end of the test.

4.3. Fracture analysis

Post-mortem fractured surface of representative samples from each tested group before and after the self-healing process is presented in Fig. 10. Fig. 10a shows a complete adhesive failure of adhesive R. The fractured surface didn't change even after the self-healing process, which can be observed in Fig. 10b. In addition, the fractured surface of adhesive R shows the yellowing phenomenon caused by the formation of carbonyl groups on the DGEBA backbone as mentioned in section 4.1.2. The yellowing is noticed in the whole fractured region because the specimens were fully opened and exposed to oxygen during the self-healing process (see Scheme 1). The uniform original brownish color was observed for adhesive A and B in Fig. 10 c-f, respectively, suggesting better thermal stability as confirmed by FTIR analysis in section 4.1.2. The penetration of the white dye, which was due to the application of a speckle pattern after the self-healing process, indicated that the specimens didn't heal enabling the easy dye penetration. Nevertheless, the self-healing process didn't cause the observable structural changes or adhesive degradation for adhesive A, while the adhesives R and B didn't show any self-healing capability.

5. Conclusions

In this study, two eco-epoxide components based on TA were synthesized: (A) glycidyl ether of TA and (B) glycidyl phosphate ester of TA and used as a replacement of the BPA-based component. The effect of modified TA component in DGEBA epoxy system on self-healing capability on Al adherends was studied. DSC analysis was performed in order to examine the residual activity and self-healing potential and it proved that adhesives have a residual reactivity at high temperatures and that adhesive A has a strong capacity for healing. FTIR indicated structural changes occurred after the high-temperature treatments and showed that R and A had the highest residual reactivity, indicating the possibility of self-healing. Furthermore, the presence of the modified TA resulted in increased thermal stability. On the other hand, DMA proved that after the treatment adhesives A and B generated polymer networks with higher cross-linking density than adhesive R. Finally, the self-healing concept was validated using SLJ testing. After the healing process, only adhesive A specimens were found to be bonded. The healing efficiency, calculated as the ratio between the healed vs. the virgin cases, from stiffness and ultimate load point of view is 90% and 50% respectively. The healed specimen has more AE events, which are generated at earlier stages in the testing, indicating the weaker mechanical bonds

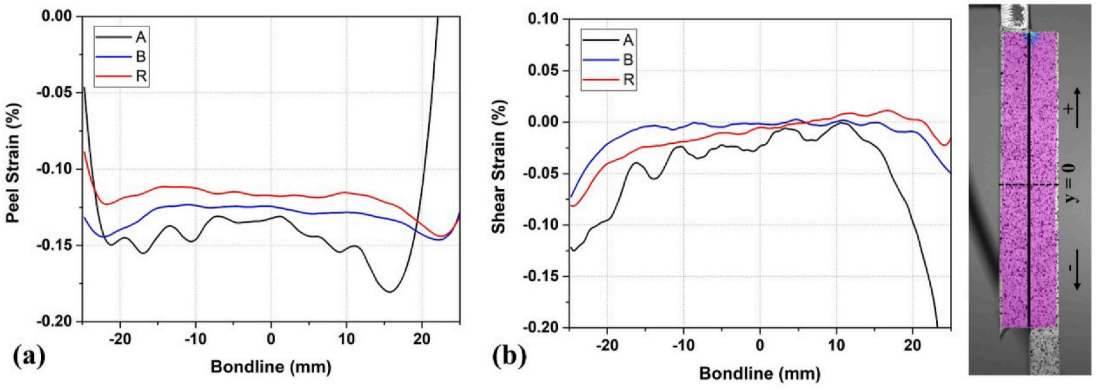

Fig. 8. Representative DIC calculated strains along the bond line: a) Peel and b) Shear.

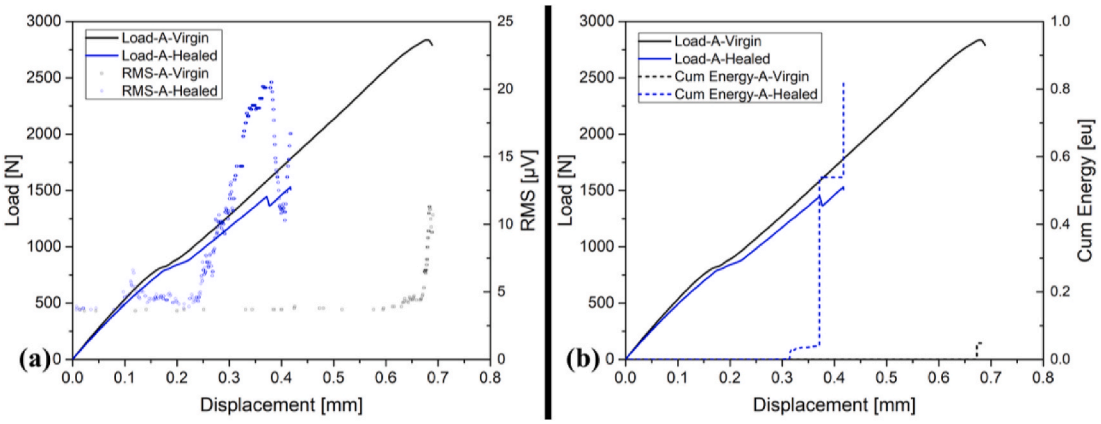

Fig. 9. Virgin vs. Healed representative load-displacement curves with AE features: a) RMS and b) Cum. Energy.

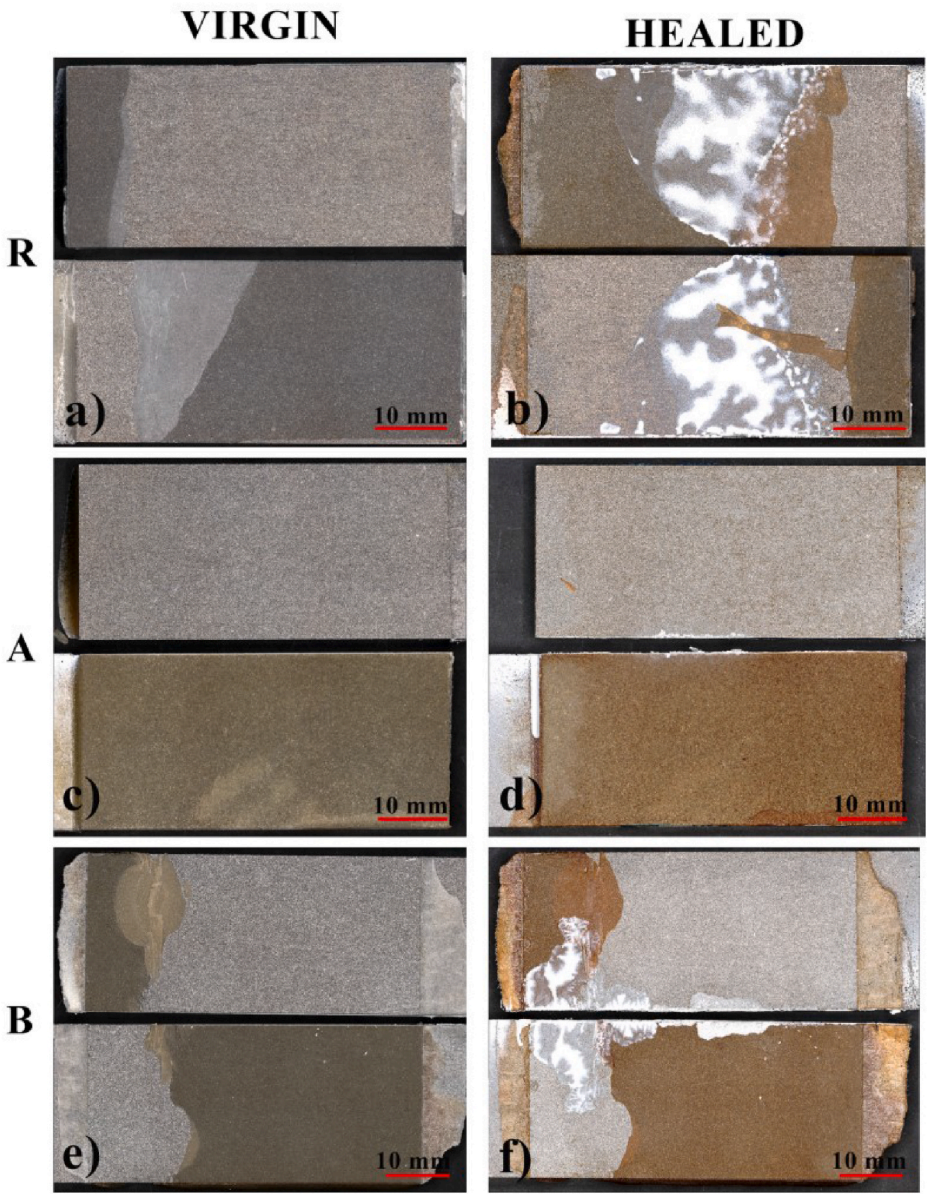

Fig. 10. Fractured surfaces of fully opened specimens before and after the self-healing process for adhesives: a) R, b) A, and c) B.

formed during the healing process. In this way, the damage is relatively more progressive, unlike the virgin case that experiences much fewer AE signals and is mainly concentrated towards the end of the test. The RMS is calculated as the root mean square of the AE signals in specific time intervals, which indicates the severity of the AE activities. In the case of adhesive A, the instantaneous increase of the RMS was observed, which referred to the macroscopic damage in the adhesive leading to the final failure of the specimen. Furthermore, the sharp increasing trend in the cumulative energy curves towards the final fracture indicated the brittle fracture nature of the adhesives. Fracture analysis was also performed before and after the self-healing process. Moreover, it did not cause the observable structural changes or adhesive degradation for adhesive A, while the adhesives R and B did not show any self-healing capability. To summarize, the self-healing concept of glycidyl ether of TA proved in this study is indicating the potential of including this component in adhesive formulations and future focus in improving the adhesive properties of this bio-based component. The main idea in that direction would be the optimization of reactivity and steric hindrance of introduced functional groups.

Acknowledgment

This publication is based upon work from COST Action CA18120 (CERTBOND - https://certbond.eu/), supported by COST (European Cooperation in Science and Technology - https://www.cost.eu/). This work was also supported by the Ministry of Education, Science and Technological Development of the Republic of Serbia (Contract No. 451-03-9/2021–14/200287 and 451-03-9/2021–14/200135).

References

[1] Thakur VK, Thakur MK, Raghavan P, Kessler MR. Progress in green polymer composites from lignin for multifunctional applications: a review. ACS Sustainable Chem Eng 2014;2:1072–92. https://doi.org/10.1021/sc500087z.
[2] Jud K, Kausch HH, Williams JG. Fracture mechanics studies of crack healing and welding of polymers. J Mater Sci 1981;16:204–10. https://doi.org/10.1007/BF00552073.
[3] Varghese S, Lele A, Mashelkar R. Metal-ion-mediated healing of gels. J Polym Sci Part A Polym Chem 2006;44:666–70. https://doi.org/10.1002/pola.21177.
[4] Yang Y, Urban MW. Self-healing polymeric materials. Chem Soc Rev 2013;42:7446. https://doi.org/10.1039/c3cs60109a.
[5] Yang Y, Ding X, Urban MW. Chemical and physical aspects of self-healing materials. Prog Polym Sci 2015;49(50):34–59. https://doi.org/10.1016/j.progpolymsci.2015.06.001.
[6] Kessler M, Sottos N, White S. Self-healing structural composite materials. Compos Part A Appl Sci Manuf 2003;34:743–53. https://doi.org/10.1016/S1359-835X(03)00138-6.
[7] Khan NI, Halder S, Goyat MS. Influence of dual-component microcapsules on self-healing efficiency and performance of metal-epoxy composite-lap joints. J Adhes 2017;93:949–63. https://doi.org/10.1080/00218464.2016.1193806.
[8] Zhu M, Liu J, Gan L, Long M. Research progress in bio-based self-healing materials. Eur Polym J 2020;129:109651. https://doi.org/10.1016/j.eurpolymj.2020.109651.
[9] White SR, Sottos NR, Geubelle PH, Moore JS, Kessler MR, Sriram SR, et al. Autonomic healing of polymer composites. Nature 2001;409:794–7. https://doi.org/10.1038/35057232.
[10] Kim JR, Netravali AN. Self-healing green composites based on soy protein and microfibrillated cellulose. Compos Sci Technol 2017;143:22–30. https://doi.org/10.1016/j.compscitech.2017.02.030.
[11] Voorhaar L, Hoogenboom R. Supramolecular polymer networks: hydrogels and bulk materials. Chem Soc Rev 2016;45:4013–31. https://doi.org/10.1039/C6CS00130K.
[12] Jethwa JK, Kinloch AJ. The fatigue and durability behaviour of automotive adhesives. Part I: fracture mechanics tests. J Adhes 1997;61:71–95. https://doi.org/10.1080/00218469708010517.
[13] Hart-Smith LJ. A peel-type durability test coupon to assess interfaces in bonded, co-bonded, and co-cured composite structures. Int J Adhesion Adhes 1999;19:181–91. https://doi.org/10.1016/S0143-7496(98)00033-5.
[14] Ghazali H, Ye L, Zhang M-Q. Lap shear strength and healing capability of self-healing adhesive containing epoxy/mercaptan microcapsules. 2016, 140004. https://doi.org/10.1063/1.4942339.
[15] Jin H, Miller GM, Pety SJ, Griffin AS, Stradley DS, Roach D, et al. Fracture behavior of a self-healing, toughened epoxy adhesive. Int J Adhesion Adhes 2013;44:157–65. https://doi.org/10.1016/j.ijadhadh.2013.02.015.
[16] Pocius AV, , Introduction, Adhes, Technol Adhes. München: Carl Hanser Verlag GmbH & Co. KG. 2012. https://doi.org/10.3139/9783446431775.001. pp. 1–15.
[17] Naito K, Onta M, Kogo Y. The effect of adhesive thickness on tensile and shear strength of polyimide adhesive. Int J Adhesion Adhes 2012;36:77–85. https://doi.org/10.1016/j.ijadhadh.2012.03.007.
[18] Grant LDR, Adams RD, da Silva LFM. Experimental and numerical analysis of single-lap joints for the automotive industry. Int J Adhesion Adhes 2009;29:405–13. https://doi.org/10.1016/j.ijadhadh.2008.09.001.
[19] Tomić NZ, Saleh MN, Teixeira de Freitas S, Živković A, Vuksanović M, Poulis JA, et al. Enhanced interface adhesion by novel eco-epoxy adhesives based on the modified tannic acid on Al and CFRP adherends. Polymers (Basel) 2020;12:1541. https://doi.org/10.3390/polym12071541.
[20] Saeedifar M, Saleh MN, De Freitas ST, Zarouchas D. Damage characterization of adhesively-bonded Bi-material joints using acoustic emission. Compos B Eng 2019;176:107356. https://doi.org/10.1016/j.compositesb.2019.107356.
[21] Saleh MN, Saeedifar M, Zarouchas D, De Freitas ST. Stress analysis of double-lap bi-material joints bonded with thick adhesive. Int J Adhesion Adhes 2019:102480. https://doi.org/10.1016/J.IJADHADH.2019.102480.
[22] Murray BR, Fonteyn S, Carrella-Payan D, Kalteremidou K-A, Cernescu A, Van Hemelrijck D, et al. Crack tip monitoring of mode I and mode II delamination in CF/Epoxies under static and dynamic loading conditions using digital image correlation. Proceedings 2018;5225. https://doi.org/10.3390/icem18-05225.
[23] Hatakeyama FXQ T. Thermal analysis fundamentals and applications to polymer science. second ed. West Sussex: John Wiley & Sons Ltd.; 1999.
[24] Tomić NZ, Marinković AD, Đ Veljović, Trifković K, Lević S, Radojević V, et al. A new approach to compatibilization study of EVA/PMMA polymer blend used as an optical fibers adhesive: mechanical, morphological and thermal properties. Int J Adhesion Adhes 2018;81:11–20. https://doi.org/10.1016/j.ijadhadh.2017.11.002.
[25] Doszlop S, Vargha V, Horkay F. Reactions of epoxy with other functional groups and the arising sec-hydroxyl groups. Period Polytech Chem Eng 1978;22:253–75.
[26] Wu Z, Li S, Liu M, Wang Z, Liu X. Liquid oxygen compatible epoxy resin: modification and characterization. RSC Adv 2015;5:11325–33. https://doi.org/10.1039/C4RA14100H.
[27] Fraga F, Vazquez EC, Rodríguez-Núñez E, Martínez-Ageitos JM. Curing kinetics of the epoxy system diglycidyl ether of bisphenol A/isophoronediamine by Fourier transform infrared spectroscopy. Polym Adv Technol 2008;19:1623–8. https://doi.org/10.1002/pat.1178.
[28] Hara O. Curing agents for epoxy resin. Three Bond Tech News 1990:1–10.
[29] Krauklis A, Echtermeyer A. Mechanism of yellowing: carbonyl formation during hygrothermal aging in a common amine epoxy. Polymers (Basel) 2018;10:1017. https://doi.org/10.3390/polym10091017.
[30] Ernault E, Richaud E, Fayolle B. Thermal oxidation of epoxies: influence of diamine hardener. Polym Degrad Stab 2016;134:76–86. https://doi.org/10.1016/j.polymdegradstab.2016.09.030.
[31] Zahra Y, Djouani F, Fayolle B, Kuntz M, Verdu J. Thermo-oxidative aging of epoxy coating systems. Prog Org Coatings 2014;77:380–7. https://doi.org/10.1016/j.porgcoat.2013.10.011.
[32] Li K, Wang K, Zhan M, Xu W. The change of thermal–mechanical properties and chemical structure of ambient cured DGEBA/TEPA under accelerated thermo-oxidative aging. Polym Degrad Stab 2013;98:2340–6. https://doi.org/10.1016/j.polymdegradstab.2013.08.014.
[33] Yousif E, Haddad R. Photodegradation and photostabilization of polymers, especially polystyrene: review. SpringerPlus 2013;2:398. https://doi.org/10.1186/2193-1801-2-398.
[34] Rosu D, Rosu L, Cascaval CN. IR-change and yellowing of polyurethane as a result of UV irradiation. Polym Degrad Stab 2009;94:591–6. https://doi.org/10.1016/j.polymdegradstab.2009.01.013.
[35] Živković A, Tomić N, Vuksanović M, Marinković A. Synthesis and characterization of epoxy resin coating with improved fire resistance by the addition of modified tannic acid. Proc. 8th Int. Conf. Renew. Electr. Power Sources, SMEITS 2020:35–42. https://doi.org/10.24094/mkoiee.020.8.1.35.
[36] Kim Y-O, Cho J, Yeo H, Lee BW, Moon BJ, Ha Y-M, et al. Flame retardant epoxy derived from tannic acid as biobased hardener. ACS Sustainable Chem Eng 2019;7:3858–65. https://doi.org/10.1021/acssuschemeng.8b04851.
[37] Zhao S, Abu-Omar MM. Renewable epoxy networks derived from lignin-based monomers: effect of cross-linking density. ACS Sustainable Chem Eng 2016;4:6082–9. https://doi.org/10.1021/acssuschemeng.6b01446.
[38] Crompton TR. Thermal methods of polymer analysis. Shawbury: Smithers Rapra Technology Ltd; 2013.
[39] Menczel JDPRB. Thermal analysis of polymers: fundamentals and applications. New Jersey: John Wiley & Sons, Inc.; 2009.
[40] Kovačević T, Rusmirović J, Tomić N, Marinović-Cincović M, Ž Kamberović, Tomić M, et al. New composites based on waste PET and non-metallic fraction from waste printed circuit boards: mechanical and thermal properties. Compos B Eng 2017;127:1–14. https://doi.org/10.1016/j.compositesb.2017.06.020.
[41] Lavoratti A, Scienza LC, Zattera AJ. Dynamic-mechanical and thermomechanical properties of cellulose nanofiber/polyester resin composites. Carbohydr Polym 2015;136:955–63. https://doi.org/10.1016/j.carbpol.2015.10.008.
[42] Kupski J, Zarouchas D, Teixeira de Freitas S. Thin-plies in adhesively bonded carbon fiber reinforced polymers. Compos B Eng 2020;184:107627. https://doi.org/10.1016/j.compositesb.2019.107627.
[43] Kupski J, Teixeira de Freitas S, Zarouchas D, Camanho PP, Benedictus R. Composite layup effect on the failure mechanism of single lap bonded joints. Compos Struct 2019;217:14–26. https://doi.org/10.1016/j.compstruct.2019.02.093.
[44] Hodgkinson JM. Testing the strength and stiffness of polymer matrix composites. In: Robinson P, Greenhalgh E, Pinho S, editors. Fail. Mech. Polym. Matrix compos. first ed. Woodhead Publishing; 2012. p. 129–82.